(10.24874/jsscm.2025.19.01.27)

SMEARED CONCEPT FOR MODELING GRADIENT-DRIVEN PROBLEMS IN COMPOSITE MEDIA (KOJIC TRANSPORT MODEL, KTM) AS A BASIS FOR BROAD APPLICATIONS

Milos Kojic[1,2*] [0000-0003-2199-5847], **Miljan Milosevic**[1,3,4] [0000-0003-3789-2404], **Vladimir Simic**[1,3] [0000-0001-7842-8902], **Bogdan Milicevic**[1,5] [0000-0002-0315-8263]

[1]Bioengineering Research and Development Center BioIRC Kragujevac, Prvoslava Stojanovica 6, 3400 Kragujevac, Serbia.
[2]Serbian Academy of Sciences and Arts, Knez Mihailova 35, 11000 Belgrade, Serbia.
[3]Institute of Information Technologies, University of Kragujevac, Department of Technical-Technological Sciences, Jovana Cvijica bb, 34000 Kragujevac, Serbia.
[4]Belgrade Metropolitan University, Tadeusa Koscuska 63, 11000 Belgrade, Serbia.
[5]Faculty of Engineering, University of Kragujevac, Sestre Janjica 6, Kragujevac 34000, Serbia
**corresponding author*

Abstract

The extremely complex biological and biochemical processes are mainly treated by laboratory and clinical investigations. In recent decades, the application of computational modeling has become more important in research and applications in the medical sciences. Despite enormous efforts and achievements in this modeling, there is still a need for new efficient and reliable methods, particularly within today's hot field – Artificial Intelligence (AI). In this report, we present a brief description of a methodology that we believe offers a basis for modeling gradient-driven physical fields in composite media, such as tissue. This methodology is based on the concept of multiscale smeared physical fields, termed the Kojic Transport Model (KTM), that is published in several journal papers and summarized in a recent book (Kojic et al. 2022). Our KTM includes modeling of partitioning, blood flow, molecular transport within the tissue, a multiscale-multiphysics model of coupling electrical field and ion concentration, and a model of convective-diffusive transport within the lung parenchyma. We present here two typical examples for the illustration of our KTM application.

Keywords: convective-diffusive transport, Kojic Transport Model, multiscale-multiphysics models, composite smeared finite element, tissue, pancreas

1. Introduction

Among many computational methods, the most generally used is the Finite Element Method (FEM), which is the basic methodology in this paper. We here provide a brief derivation of the Kojic Transport Model (KTM), which is based on the smeared concept of physical gradient-driven fields, and we indicate its generality regarding application in biomedical engineering. As discussed in our paper (Kojic et al. 2024), the KTM has a strong distinction from other approaches; other approaches are given in references (Koh et al. 2003, Hyde et al. 2013a, Hyde et al. 2013b, Di Gregorio et al. 2019, Corrias et al. 2012) and compared with our KTM. Inspiration for the formulation of the KTM was the task of how to model in a simple, robust, and applicable manner mass transport in a tissue, composed of a capillary system, extracellular space, and cells; with, the possible inclusion of the biological processes within cells.

In the next section, we summarize the basic concept of the KTM by the derivation of the fundamental equations of our Composite Smeared Finite Element (CSFE). Then, we show two typical examples of the application of the KTM, and give concluding remarks in the final section.

2. Formulation of the Composite Smeared Finite Element (CSFE)

Here we summarize the FE formulation according to (Kojic 2018) . Application of this methodology is given in a number of our references (Kojic et al. 2017a, 2017b, 2017d, 2018a, 2018b, 2019 and Milosevic et al. 2018a, 2018b, 2020), while the complete summary is provided in (Kojic et al. 2022) . The KTM is implemented in our FE software package PAK, the modulus PAK-KTM (Kojic et al. 2006).

The first step in the derivation of the smeared concept is to transform the 1D flow and mass transport within capillaries into a continuum form. Following the illustration in Fig. 1, we can write the following relation:

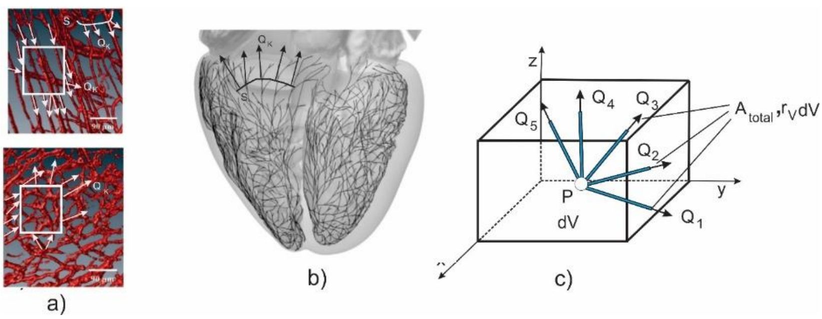

Fig. 1 Illustration of the transformation of the 1D flow to a 3D form, a first step in the formulation of the KTM. a) Capillary system and blood flow through a representative domain. b) Electrical conduction through the Purkinje network in the heart. c) A representative volume of the continuum in the vicinity of the space point P. (according to Kojic et al. 2022)

$$A_{tot}\mathbf{q}_{cont} = \sum_K \mathbf{Q}_K = -\sum_K D_K A_K \frac{\partial \phi_K}{\partial x_K} \ell_{Ki} \mathbf{i}_i, \quad \text{sum on } i\text{: } i = 1,2,3 \tag{1}$$

where for the K-th 1D element we have: A_K is the cross-sectional area, Q_K is the flux through the surface A_K, D_K is the transport coefficient; $\phi_K = \phi$ is the value of the field ϕ – the same for all 1D structures (assuming that they are interconnected) in a small surrounding of a continuum spatial point P; x_K is the axial coordinate, ℓ_{Ki} are projections of the axial unit vectors i_i ;

$$A_{tot} = \sum_K A_K \tag{2}$$

is the total area of all cross-sectional areas A_K; and q_{cont} is flux as the amount of the transported physical quantity per unit time through the surface A_{tot}. We here assume the gradient-driven flow within the 1D structures, i.e.

$$\mathbf{Q}_K = -D_K A_K \frac{\partial \phi_K}{\partial x_K}, \quad \text{no sum on } K \tag{3}$$

Further, we have that

$$\frac{\partial \phi_K}{\partial x_K} = \frac{\partial \phi}{\partial x_j} \ell_{Kj}, \quad \text{no sum on } K; \ \text{sum on } j\text{: } j=1,2,3 \tag{4}$$

and then, substituting to (1), we have

$$\mathbf{q}_{cont} = -\frac{1}{A_{tot}} \frac{\partial \phi}{\partial x_j} \sum_K D_K A_K \ell_{Ki} \ell_{Kj} \mathbf{i}_i = -D_{ij} \frac{\partial \phi}{\partial x_j} \mathbf{i}_i; \quad \text{or} \quad \left(\mathrm{q}_{cont}\right)_i = -D_{ij} \frac{\partial \phi}{\partial x_j} \tag{5}$$

where

$$D_{ij} = \frac{1}{A_{tot}} \sum_K D_K A_K \ell_{Ki} \ell_{Kj} \tag{6}$$

is the transport tensor representing all 1D structures. This form of the transport tensor was derived analogously in references (Dimkic et al. 2013, Kojic et al. 2017, Milosevic et al. 2018) for diffusion and fluid transport through porous media and mass release from nanofibers.

Looking at a composite medium, we have different domains with their continuum physical fields which are mutually interdependent. In the formulation of our continuum finite element, we introduce connectivity elements. So, the next step is to formulate connectivity as follows. In analogy with our connectivity elements in (Dimkic et al. 2013), we introduce the connectivity elements at each FE node. Fig. 2b shows a connectivity element at node B between the 1D element and continuum. According to Fig. 2a, we have that the elementary flux dQ_w is

$$dQ_w = -D_w dA_{surface}\left(\phi_{1D} - \phi_{sur}\right) = -D_w dA_{surface}\left(\phi_1 - \phi_2\right) = -D_w r_{AV} r_V dV\left(\phi_{1D} - \phi_{sur}\right) \tag{7}$$

where $dA_{surface}$ is the elementary surface, dV is the elementary volume of the continuum; r_{AV} and r_V are the volumetric fraction and the area-to-volume ratio of the 1D structure, respectively; D_w is the transport coefficient through the wall of the thickness h; and ϕ_{1D} and ϕ_{sur} are values of the physical field in the 1D space and 3D surrounding. Then, for a node J of the finite element mesh and linear interpolation functions, we have the following equilibrium equation of the connectivity element, for a time step of the size Δt and iteration i:

$$\left(\frac{1}{\Delta t}M_{IJ}+K_{IJ}^{w}\right)\Delta\phi^{J(i)}=-\left(\frac{1}{\Delta t}M_{IJ}+K_{IJ}^{w}\right)\phi^{J(i-1)}+\frac{1}{\Delta t}M_{IJ}\phi^{Jt},\quad I,J=1,2 \tag{8}$$

where the matrices M and K^w can be expressed as

$$\begin{aligned}&M_{11}=M_{22}=\frac{1}{3}cr_{AV}r_{V}V_{J}\,,\quad \mathrm{M}_{12}=\mathrm{M}_{21}=\frac{1}{6}cr_{AV}r_{V}V_{J}\\&K_{11}^{w}=K_{22}^{w}=-K_{12}^{w}=-K_{21}^{w}=D_{w}r_{AV}r_{V}V_{J}\end{aligned} \tag{9}$$

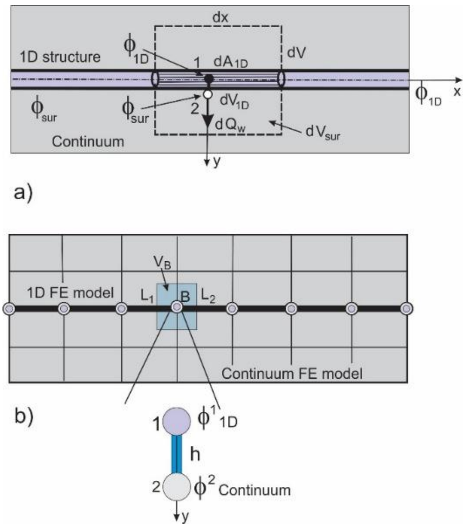

Fig. 2 Geometrical interpretation of the formulation of the connectivity element between 1D and 3D surrounding. a) Elementary flux dQ_w through the surface dA_{1D} to the surrounding of the volume dV_{sur}. b) Connectivity element with the length h corresponding to the volume of the continuum V_B. (according to Kojic, et al., 2022).

where c is the rate coefficient. The material parameters of this element, c and D_w, represent the characteristics of the wall and can include various biological properties important in modeling biological barriers; they are used in our models built in the PAK-KTM software package (Kojic et al. 2006).

Now, we can formulate our Composite Smeared Finite Element (CSFE) shown in Fig. 3. We have the continuum domains composed of different physical fields, occupying the corresponding volumetric fractions, which include the 1D domains represented by the continuum form with the transport tensors (6). The domains are mutually coupled by the connectivity elements satisfying the balance equations (8). The balance equations for the continuum domains can be written as

$$\left(\frac{1}{\Delta t}\mathbf{M}+\mathbf{K}\right)^{(i-1)}\Delta\mathbf{\Phi}^{(i)}=\mathbf{Q}^{ext(i-1)}+\mathbf{Q}_{V}^{(i-1)}-\left(\frac{1}{\Delta t}\mathbf{M}+\mathbf{K}\right)^{(i-1)}\mathbf{\Phi}^{(i-1)}+\frac{1}{\Delta t}\mathbf{M}\mathbf{\Phi}^{t} \tag{10}$$

where the element matrices M and K take into account transitional and transport characteristics, while $\mathbf{Q}^{ext(i-1)}$ and $\mathbf{Q}_V^{(i-1)}$ are external (to the element) and volumetric fluxes; and $\mathbf{\Phi}^{(i)}$, $\Delta\mathbf{\Phi}^{(i)}$ and $\mathbf{\Phi}^t$ are nodal vectors, nodal increments, and vectors at the start of a time step, respectively. The matrices include the volumetric fractions of the domains. For example, the transport matrix K for a domain K is

$$K_{IJ}^K = \int_V r_V^K D_{ij}^K \frac{\partial N_I}{\partial x_i} \frac{\partial N_J}{\partial x_j} dV, \quad sum\ on\ i, j;\ i, j = 1, 2, 3 \tag{11}$$

where r_V^K is the volumetric fraction, and N_I, N_J are the FE interpolation functions.

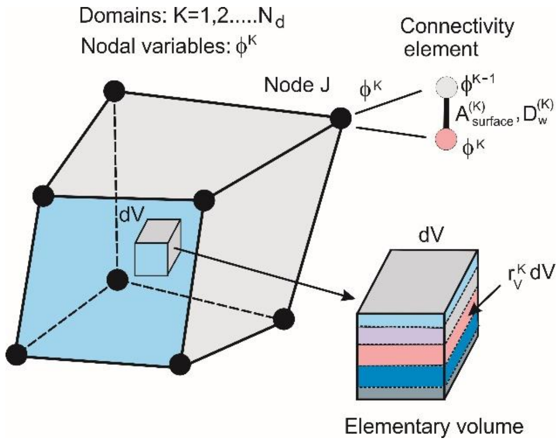

Fig. 3 Composite Smeared Finite Element (CSFE) with coupled physical fields within volumetric domains occupying the element space. According to (Kojic et al, 2022).

The connectivity elements are practically fictitious elements representing biological barriers as capillary walls or cell membranes. The balance equation for a connectivity element at node J between domains m and n is (neglecting the rate terms)

$$K_{wIJ}^{m,n} \Delta\Phi_J = -K_{wIJ}^{m,n} \Phi_J, \quad I, J = 1, 2 \tag{12}$$

where the connectivity matrix $K_{wIJ}^{m,n}$ is

$$K_{wIJ}^{m,n} = r_V r_{AV} D_w V_{node} \begin{bmatrix} 1 & -1 \\ -1 & 1 \end{bmatrix} \tag{13}$$

In the above equations, r_V, r_{AV}, D_w and V_{node} are the nodal values of the volumetric fraction, area-to-volume coefficient, wall transport coefficient, and volume (of the continuum) belonging to the node, respectively. We have that the area coefficient is $r_{AV} = 4/d_{cap}$ for capillaries with d_{cap} being the capillary diameter, while for spherical cells with diameter $d_{cell,}$ it is $r_{AV} = 6/d_{cell}$. It is important to emphasize that various characteristics of the biological barriers (capillary walls, cell membranes), such as partitioning or effects of ionic transport, are represented by the connectivity elements.

3. Examples

Among a large number of examples in our references, we select two characteristic ones, one to illustrate the accuracy of the KTM solutions, and the other to show applicability to large models.

3. 1. Diffusion within tissue sample taken from a pancreatic tumor

A small tissue sample 50x50 micron size, shown in Fig. 4a, is taken from images of pancreas cancerous tissue (E. J. Koay, MD Anderson Cancer Center, Houston). We have assumed that there are two types of cells, with different cytosol properties, and with three organelles within each cell. It is assumed that there are 6 capillaries normal to the plane of the model, with a prescribed concentration. We consider two FE models, the detailed model – in Fig. 4c, and the smeared model – in Fig. 4d. As shown in the figure, there is a large difference in the number of equations between the two models. Model geometrical data are (lengths in microns): Capillaries: 5, Diameter $d_{mean} = 3.97$, wall thickness = 0.62, vol fraction $r_V = 0.0247$; Tissue: 50x50, $A_{total} = 2500$, $A_{tissue} = (1 - 0.0247) * A_{total} = 2438$; Cell 1 (24): $r_V = 0.307$, $d_{mean} = 6.30$; Organelles: 1) $r_V = 0.334$, $d_{mean} = 3.64$; 2) $r_V = 0.034$, $d_{mean} = 1.16$; 3) $r_V = 0.03$, $d_{mean} = 1.10$; Cell 2 (21): $r_V = 0.257$, $d_{mean} = 6.16$; Organelles: 1) $r_V = 0.257$, $d_{mean} = 3.17$; 2) $r_V = 0.051$, $d_{mean} = 1.39$; 3) $r_V = 0.056$, $d_{mean} = 1.46$.

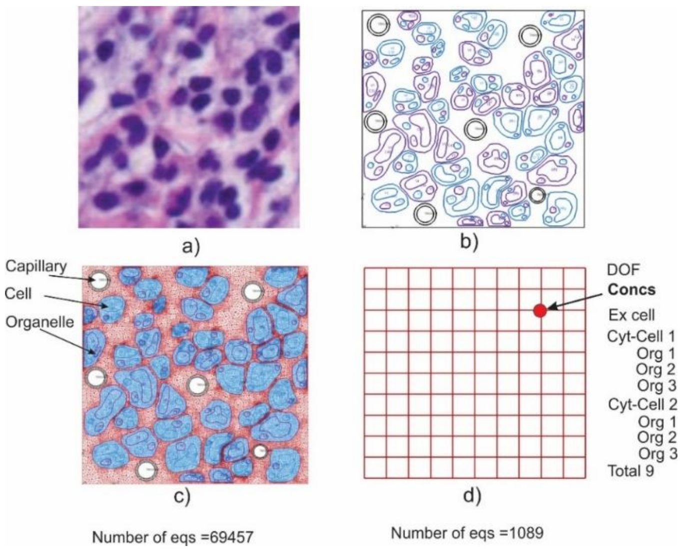

Fig. 4 2D model of diffusion within tissue. a) Image of pancreatic cancer tissue; b) Contours of capillaries, cells and organelles; c) Detailed model with 2D elements; d) Smeared model (KTM) with nodal concentrations to be calculated (concentrations in capillary domain are prescribed). (according to Kojic et al., 2022)

It is assumed that the two cell types occupy separate domains; the boundaries of the two cell groups are shown by black and dark lines in Fig. 5b. It is assumed that concentration within capillaries is constant (a bolus type is considered in Kojic et al. 2022). Also, different diffusivities and partitioning are assumed. We presume that wall diffusivities are the same for tissue and the medium (for capillaries as in extracellular space, for cells as in cytosol, and organelles as within organelles). It is taken that diffusion coefficients are the same in all compartments and the walls, D=100[μ^2/s]; while concentrations are given in [M].

We assume that there is hydrophobicity, expressed the partitioning, at the cell membrane and organelle membranes of cell group 2. We consider two cases, with partitioning P=10 and P=0.1. The evolution of the mean concentration for four compartments is shown in Figs. 5a, while the concentration field at time t=0.5s and diagram of the ultimate concentration along the central axis *x* are shown in Figs. 5b,c. It can be seen that concentration discontinuities occur at membranes with partitioning. Besides the fact that there is a very heterogeneous field of concentration shown in the figure, obtained by the detailed model, there is quite a good agreement between mass accumulation within compartments for the detailed and the KTM model. Detailed discussion of the results is given in (Kojic et al. 2022).

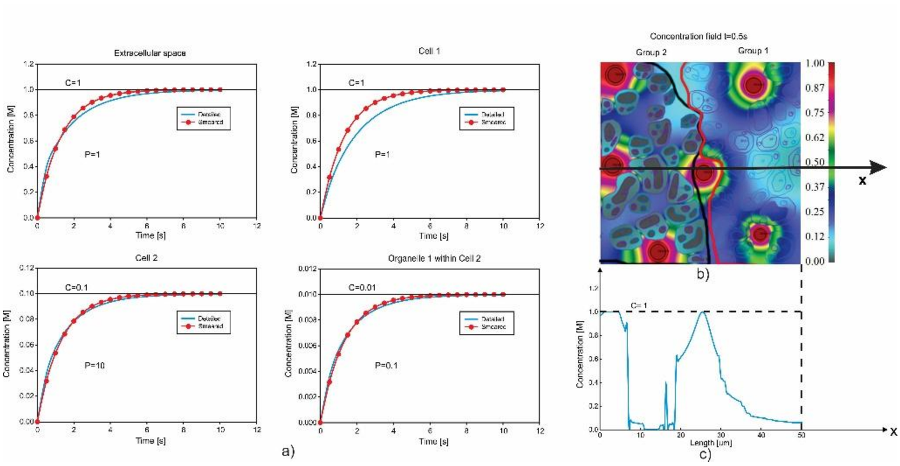

Fig. 5 Diffusion from capillaries, with constant concentration C=1, to tissue with two groups of cells, Cell 1 and Cell 2. Diffusivities are the same in all compartments D=100, while partitioning for cell membranes is: P=1 for Cell 1 and its organelles, and P=10 for Cell 2 and its organelles. a) Mean concentration evolution in four compartments. b) Concentration field at time t=0.5s; c) Diagram of ultimate concentration along the axis *x*. (according to Kojic et al. 2022)

3.2. Diffusion within the pancreas

This example demonstrates the application of the KTM to large-scale models. In (Kojic et al. 2022 and 2018a), it was considered mass transport in the pancreas when a bolus-type is injected within the entrance of the main artery of the pancreas. It is assumed the pressure is constant at the entrance. We used imaging data obtained at a lab in the MD Anderson Cancer Center in Houston. The mode consists of: large blood vessels, capillary system, lymphatic system, extracellular space, and two types of cells with their organelles. Altogether, we have 7 continuum subdomains with their volumetric fractions, diffusion characteristics, and partitioning at cell and organelle membranes. Each node has 10 variables – 3 pressures and 7 concentrations. The number of equations to be solved is 1,025,502. Other details are given in the reference (Kojic et al. 2018a and 2022). Fig. 6 displays concentration fields in different domains, where differences can be noticed due to partitioning effects. Fig. 7 shows the evolution of the mean concentration in different domains which also demonstrates the effects of the diffusion and partitioning characteristics.

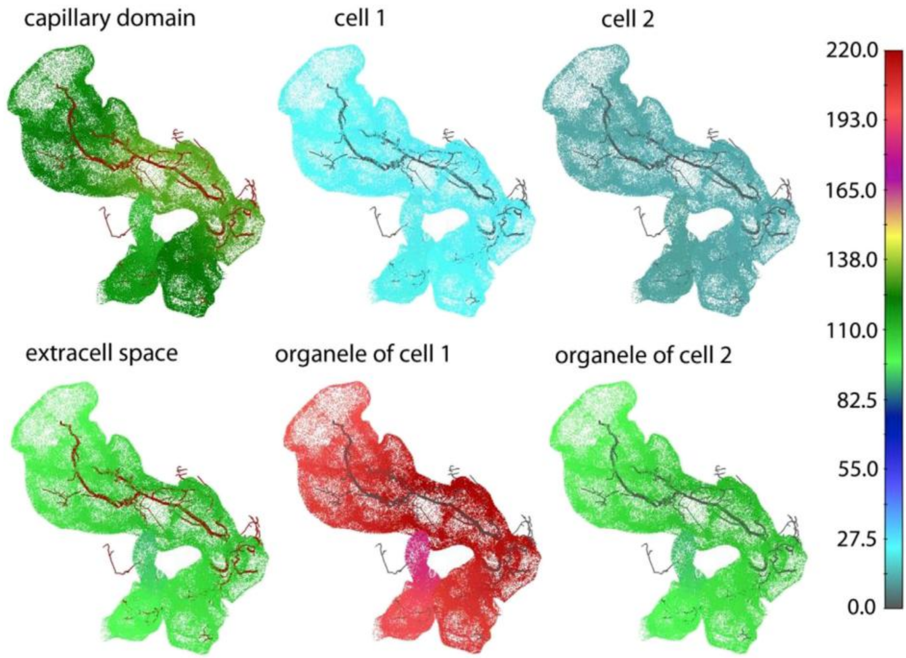

Fig. 6. Concentration fields within the pancreas at time t = 20s. Concentration for the Cell 2 group (portioning P = 10 at cell membrane) is significantly smaller than for Cell 1 (P =5) due to partitioning. (According to Kojic, et al 2018a and 2022) .

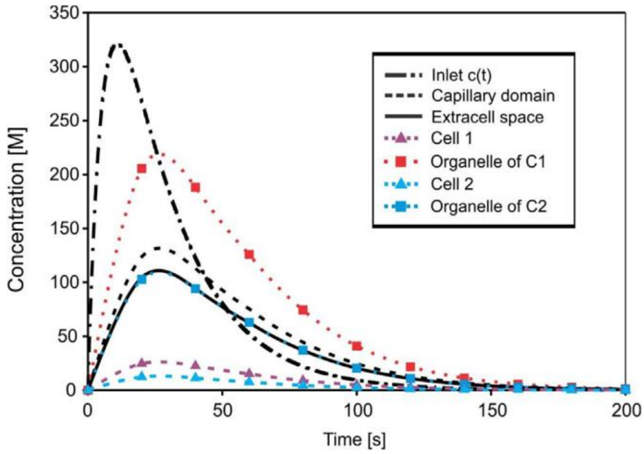

Fig. 7. Evolution of concentration in different domains of the pancreas. (According to Kojic, et al. 2018b and 2022)

4. Concluding remarks

This summary serves as a description of our smeared concept for the finite element modeling of the gradient-driven physical fields. This methodology is termed the Kojic Transport Model (KTM). We believe that, due to the generality of the KTM, it can be applied to medicine, biology, and science to model various complex multiscale and multiphysics problems. The accuracy of the KTM is illustrated on two characteristic examples from our earlier publications. The first example demonstrates the efficiency and accuracy of the KTM. The second example serves to show the applicability of the KTM to large-scale models, with a true multiscale description. The FE model of the entire pancreas is generated from images, and it includes large vessels, extracellular space, capillary and lymphatic systems, and two groups of cells with their organelles and hydrophobic properties of transported molecules.

It can be concluded that the KTM, due to its generality, ease, straightforward application, accuracy, and efficiency, can serve as a tool in the development of today's important expert systems within AI and for everyday medical practice.

Acknowledgments. This research was funded by the Ministry of Education, Science and Technological Development of the Republic of Serbia, contract numbers [451-03-68/2022-14/200107 (Faculty of Engineering, University of Kragujevac), 451-03-68/2022-14/200378 (Institute for Information Technologies Kragujevac, University of Kragujevac); grant number F-134 (Serbian Academy of Sciences and Arts). The authors are thankful to the City of Kragujevac, Serbia.

References

Kojic M, Milosevic M, Ziemys A (2022). Computational Models in Biomedical Engineering - Finite Element Models Based on Smeared Physical Fields: Theory, Solutions, and Software, Elsevier.

Kojic M, Milosevic M, Simic V, Milicevic B, Terracciano R, Filgueira CS (2024). On the generality of the finite element modeling physical fields in biological systems by the multiscale smeared concept (Kojic Transport Model), Heliyon, 10, e263.

Koh TS, Cheong LH, Hou Z, Soh YC (2003). A physiologic model of capillary–tissue exchange for dynamic contrast-enhanced imaging of tumor microcirculation, IEEE Trans. Biomed. Eng., 50(2), 159-167.

Hyde ER, Cookson AN, Lee J, Michler C, Goyal A, Sochi T, Chabiniok R, Sinclair M, Nordsletten DA, Spaan J, van den Wijngaard JPHM, Siebes M, Smith NP (2013a). Multi-scale parameterisation of a myocardial perfusion model using whole-organ arterial networks, Ann. Biomed. Eng., DOI: 10.1007/s10439-013-0951-y.

Hyde ER, Michler C, Lee J, Cookson AN, Chabiniok R, Nordsletten DA, Smith NP (2013b). Parameterisation of multi-scale continuum perfusion models from discrete vascular networks, Med. Biol. Eng. Comput., 51, 557–570.

Di Gregorio S, Fedele M, Pontone G, Corno AF, Zunino P, Vergara C, Quarteroni A (2019). A multiscale computational model of myocardial perfusion in the human heart, MOX, Dipartimento di Matematica, Politecnico di Milano.

Corrias A, Pathmanathan P, Gavaghan DJ, Buista ML (2012). Modelling tissue electrophysiology with multiple cell types: applications of the extended bidomain framework, Integr. Biol., 4, 192–201.

Kojic M (2018). Smeared concept as a general methodology in finite element modeling of physical fields and mechanical problems in composite media, J. Serb. Soc. Comp. Mech., 12(2), 1-16.

Kojic M, Milosevic M, Simic V, Koay EJ, Fleming JB, Nizzero S, Kojic N, Ziemys A, Ferrari M (2017a). A composite smeared finite element for mass transport in capillary systems and biological tissue, Comput. Methods Appl. Mech. Eng., 324, 413–437. https://doi.org/10.1016/j.cma.2017.06.019

Kojic M, Milosevic M, Simic V, Koay EJ, Kojic N, Ziemys A, Ferrari M (2017b). Extension of the Composite Smeared Finite Element (CSFE) to include lymphatic system in modeling mass transport in capillary systems and biological tissue, J. Serb. Soc. Comp. Mech., 11(2), 108-120.

Kojic M, Simic V, Milosevic M (2017c). Composite smeared finite element – some aspects of the formulation and accuracy, IPSI Trans. Adv. Res., 13(2), 2017.

Kojic M, Milosevic M, Simic V, Stojanovic D, Uskokovic P (2017d). A radial 1D finite element for drug release from drug loaded nanofibers, J. Serb. Soc. Comp. Mech., 11(1), 82-93.

Kojic M, Milosevic M, Kojic N, Koay EJ, Fleming JB, Ferrari M, Ziemys A (2018a). Mass release curves as the constitutive curves for modeling diffusive transport within biological tissue, Comput. Biol. Med., 92, 156–167. DOI: 10.1016/j.compbiomed.2016.06.026.

Kojic M, Milosevic M, Simic V, Koay EJ, Kojic N, Ziemys A, Ferrari M (2018b). Multiscale smeared finite element model for mass transport in biological tissue: from blood vessels to cells and cellular organelles, Comput. Biol. Med., 99, 7–23. https://doi.org/10.1016/j.compbiomed.2018.05.022

Kojic M, Milosevic M, Simic V, Ziemys A, Filipovic N, Ferrari M (2019). Smeared multiscale finite element model for electrophysiology and ionic transport in biological tissue, Comput. Biol. Med., 108, 288–304.

Milosevic M, Simic V, Milicevic B, Koay EJ, Ferrari M, Ziemys A, Kojic M (2018a). Correction function for accuracy improvement of the Composite Smeared Finite Element for diffusive transport in biological tissue systems, Comput. Methods Appl. Mech. Eng., https://doi.org/10.1016/j.cma.2018.04.012

Milosevic M, Stojanovic D, Simic V, Milicevic B, Radisavljevic A, Uskokovic P, Kojic M (2018b). A computational model for drug release from PLGA implant, Materials, 11(12), 2416. https://doi.org/10.3390/ma11122416

Milosevic M, Stojanovic DB, Simic V, Grkovic M, Bjelovic M, Uskokovic PS, Kojic M (2020). Preparation and modeling of three-layered PCL/PLGA/PCL fibrous scaffolds for prolonged drug release, Sci. Rep., 10(1), 11126. DOI: 10.1038/s41598-020-68117-9. Erratum in Sci. Rep., 11(1), 16028, 2021.

Kojic M, Filipovic N, Milosevic M (2006). PAK-KTM: Finite Element Program for Bioengineering Problems, Bioengineering R&D Center and University of Kragujevac, Serbia.

Kojic M (2020). Multiscale composite 3D finite element for lung mechanics, J. Serb. Soc. Comp. Mech., 14(1), 1-11.

Kojic M, Milosevic M, Wu S, Blanco E, Ferrari M, Ziemys A (2015). Mass partitioning effects in diffusion transport, Phys. Chem. Chem. Phys., 17, 20630-20635.

Kojic M (2023). A multiscale multiphysics finite element for lung, J. Serb. Soc. Comp. Mech., 17(2), 1-15.

Terracciano R, Milicevic B, Milosevic M, Simic V, Carcamo-Bahena Y, Royal ALR, Carcamo-Bahena AA, Butler EB, Grattoni A, Kojic M, Filgueira CS (2023). An insight into perfusion anisotropy within solid murine lung cancer tumors, to be submitted.

Dimkic M, Rankovic V, Filipovic N, Stojanovic B, Isailovic V, Pusic M, Kojic M (2013). Modeling of radial well lateral screens using 1D finite elements, J. Hydroinformatics, 15(2), 405-415.